Prandtl number dependence of the viscous boundary layer and the Reynolds numbers in Rayleigh-Bénard convection

Siu Lam, Xiao-Dong Shang, Sheng-Qi Zhou, and Ke-Qing Xia*
Department of Physics, The Chinese University of Hong Kong, Shatin, Hong Kong, China
(Received 8 January 2002; published 24 June 2002)

We report results from high Prandtl number turbulent thermal convection experiments. The viscous boundary layer and the Reynolds number are measured in four different fluids over wide ranges of the Prandtl number Pr and the Rayleigh number Ra, all in a single convection cell of unity aspect ratio. We find that the normalized viscous layer thickness may be represented as $\delta_v/L = 0.65\mathrm{Pr}^{0.24}\mathrm{Ra}^{-0.16}$. The Reynolds number based on the oscillation frequency of the large-scale flow is found as $\mathrm{Re}_o(\mathrm{Ra},\mathrm{Pr}) = 1.1\mathrm{Ra}^{0.43}\mathrm{Pr}^{-0.76}$ and that based on the rms velocity $\mathrm{Re}_{rms}(\mathrm{Ra},\mathrm{Pr}) = 0.84\mathrm{Ra}^{0.40}\mathrm{Pr}^{-0.86}$. Both the Ra and the Pr exponents of $\mathrm{Re}_{V_m}(\mathrm{Ra},\mathrm{Pr})$ based on the maximum velocity of the circulating wind appear to vary across the range of Pr covered, changing from 0.5 to 0.68 and -0.88 to -0.95, respectively, as Pr is increased from 6 to 1027.

DOI: 10.1103/PhysRevE.65.066306 PACS number(s): 47.27.Te, 05.40.−a

I. INTRODUCTION

The complex nature of the Rayleigh-Bénard convection problem often means that theoretical models that are able to produce experimentally observed scaling laws for a few global and local quantities do not necessarily provide the right mechanism for turbulent motion in the system. It is thus important that a comprehensive approach be taken which considers how the system's response parameters (i.e., Nu and Re) are dependent on its control parameters (i.e., Ra and Pr) in a systematic way [1]. In contrast to the Nusselt number Nu, which has been measured over wide ranges of the Rayleigh number Ra [2] and the Prandtl number Pr [3], the experimentally measured Reynolds numbers generally span rather narrow ranges of the control parameters. This is especially true with regard to the Prandtl number. Because any Prandtl number dependence of Nu is likely to be weak and that of Re has been predicted to be strong by many theories, measurement of the Reynolds number may provide a more sensitive test for the various models. Another quantity of importance is the viscous boundary layer. Because the various models all make specific assumptions about the viscous boundary layer δ_v, determination of δ_v may allow us to better discriminate the different mechanisms proposed. Here again, experiment appears to lag behind. To our knowledge, directly measured δ_v exist only for a single Pr (water) [4,5]. For other values of Pr, there are results obtained with the indirect ''power spectra'' method [6,7], but there have been questions about the validity of this method [8]. Thus, measuring the viscous boundary layer and the Reynolds number over a wide range of Pr and Ra should provide us the much-needed information.

In this paper, we report an experimental study of high-Prandtl-number turbulent Rayleigh-Bénard convection in which both the viscous boundary layer $\delta_v(\mathrm{Ra},\mathrm{Pr})$ and the Reynolds number $\mathrm{Re}(\mathrm{Ra},\mathrm{Pr})$ are measured as functions of Ra and Pr. The paper is organized as follows. Section II contains a brief description of the working fluids, the convection cell, and the velocity measurements. Section III is divided into four parts: (a) Velocity profiles at various values of Ra and Pr, the measured viscous boundary layer, and its comparison with indirectly measured results for low-Pr fluids. (b) The Reynolds number based on the maximum values of vertical profiles of the horizontal velocity component; previously obtained results from water in several cells of various aspect ratios are also reanalyzed here. (c) The Reynolds number based on the oscillation frequency of the large-scale mean flow. (d) The Reynolds number based on the rms values of local velocity. We summarize our findings in Sec. IV.

II. EXPERIMENT

Three alcohol-type organic liquids, 1-pentanol, triethylene glycol, and dipropylene glycol [9], plus water are used as convecting fluids. The Rayleigh and Prandtl numbers are calculated based on temperatures measured at the center of the convection cell [10] and using recently published properties of the fluids [11]. With these fluids, we achieve a combined range of Ra from 1×10^8 to 3×10^{10} and of Pr from 3 to 1205, all in a single convection cell of unity aspect ratio. The convection cell has been described in detail elsewhere [12] and only its key features will be mentioned. Briefly, it is a vertical cylinder with diameter D and height L both equal to 19 cm, with gold-plated copper conducting plates, and a Pyrex glass tube as sidewall. Local velocities in the bulk region are measured using the laser Doppler velocimetry (LDV) technique. In the present work, a commercial LDV (Dentac Ltd.) is used to measure the local vertical velocity near sidewall. The LDV has a measuring volume of about 75 μm and continuous acquisition of the local fluctuating velocity can be made for many hours. Near the bottom plate where the viscous boundary layer is to be measured, strong temperature fluctuations cause strong fluctuations of the refractive index, which significantly reduce the signal to noise ratio of the LDV and thus limit its use in that region. To overcome this, we used dual-beam incoherent cross-correlation spectroscopy [13] to determine δ_v. This technique has been shown to be effective for boundary layer

*Corresponding author. Email address: kxia@phy.cuhk.edu.hk

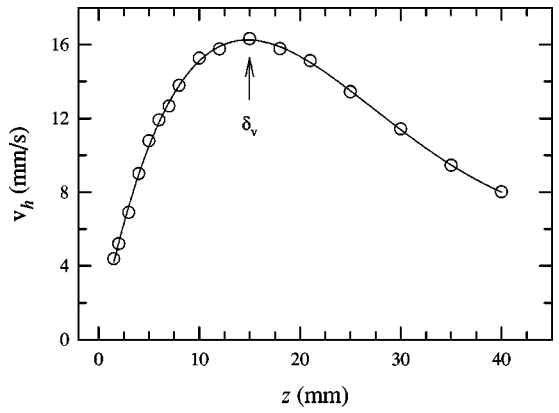

FIG. 1. Mean horizontal velocity as a function of the distance from the bottom plate, at Ra $=4.1\times10^9$ and Pr $=298$. The curve is a polynomial fit for determining the maximum velocity.

measurement in thermal convection and its application in turbulent convection has been well documented [4,5,14]. To scatter light, we seeded water with neutrally buoyant latex spheres and the three organic liquids with hollow glass spheres that are density matched for each of the fluids [15].

III. RESULTS AND DISCUSSION

A. The viscous boundary layer

Figure 1 shows a profile of the horizontal velocity v_h measured from the lower plate along the central axis at Ra $=4.1\times10^9$ and Pr $=298$ (dipropylene glycol). The profile, if extrapolated to $z=0$, would be downward concave [16] and this may be understood in terms of a constant viscous stress (rather than constant shear) boundary condition for non-Boussinesq convection [17,18]. Thus convection at some of the large Pr values may be non-Boussinesq; nonetheless we shall see below that certain features appear to be ''universal'' across the wide range of Pr covered in our experiment. Because of the lack of a linear region in the velocity profile, we adopt an operational definition for the viscous layer thickness δ_v different from the one previously used in water [4]. We take the position of the maximum velocity as δ_v. In Fig. 1, the solid curve is a polynomial fit to the data, which yields δ_v. Another interesting thing to note is that profiles for different values of Ra but the same Pr appear to have an invariant form, whereas those of different Pr but of approximately the same Ra do not seem to have the same shape. These are shown, respectively, in Figs. 2(a) and 2(b) in scaled form. As will be seen below, horizontal profiles of the vertical velocity component measured near the sidewall also show Pr-dependent shapes. Note that a universal form for velocity profiles having different Ra and approximately the same Pr has been observed previously [4], but, to our knowledge, no information is available on the Prandtl number properties of the velocity profiles.

In Fig. 3(a) we plot the measured viscous boundary layer thickness δ_v vs Ra for three values of the Prandtl number: 51 (triangles, 1-pentanol), 298 (inverted triangles), and 1030 (squares) (both dipropylene glycol); the circles are a previous result [4] measured in water with Pr $=6$ (for consistency,

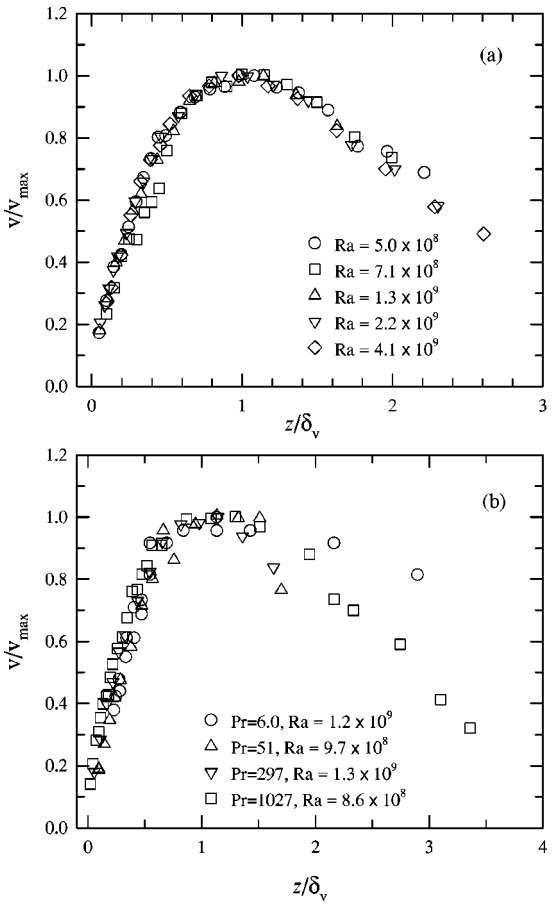

FIG. 2. (a) Scaled velocity profiles for five values of Ra but the same Pr $=298$. (b) Scaled velocity profiles of approximately the same Ra but different Pr.

reanalyzed using the new definition, which resulted in a roughly factor of 2 increase in the magnitude of δ_v for all values of Ra). All the data may be described by the power-law fit $\mathrm{Ra}^{0.16}$, which is represented by the lines in the figure. This result is consistent with the previous findings in water using the ''old'' definition [4,5]. With the Ra dependence determined, we examine the Pr-dependent amplitude $A(\mathrm{Pr}) = \delta_v \mathrm{Ra}^{0.16}$. The result is plotted as a function of Pr in Fig. 3(b) where the line is a power-law fit:

$$\delta_v/L = 0.65\mathrm{Ra}^{-0.16\pm0.02}\mathrm{Pr}^{0.24\pm0.01}. \quad (1)$$

With both the Prandtl number and Rayleigh number dependences of the viscous boundary layer established over a wide range, we examine the possibility of applying it to systems of very different Pr values such as those of gas and mercury, where direct measurements are not yet possible but indirect measurements have been made [6,7]. The indirect technique is based on a coincidence between the peak positions of the spatial profile of the cutoff frequency of the temperature power spectrum and the profile of the velocity [6]. Because the coincidence was observed at a single value of Ra and of Pr (water), the generalization of this method contains two assumptions: (1) the coincidence will hold for other values of Ra, and (2) it will hold for other values of Pr. Furthermore,

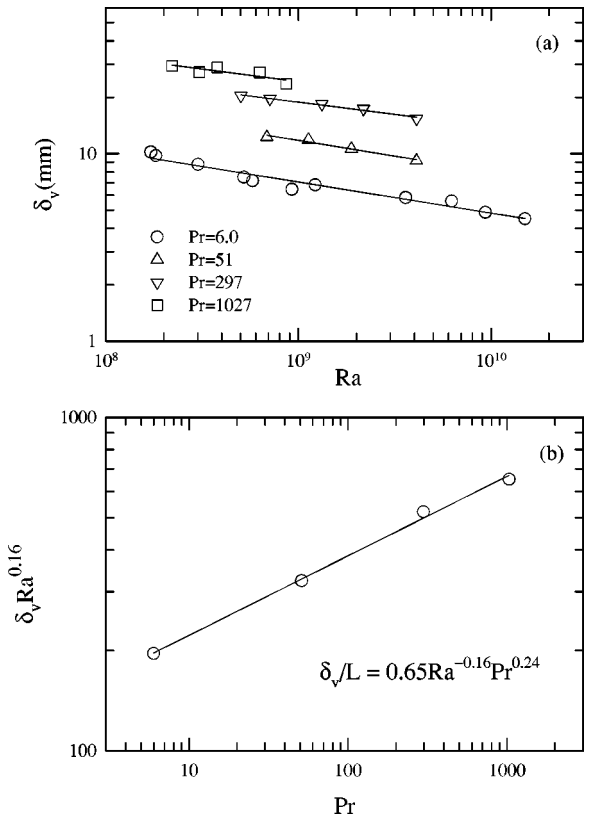

FIG. 3. (a) Viscous boundary layer δ_v vs Ra for four values of Pr. (b) Pr dependence of the viscous boundary layer; the fitting line represents $\delta_v/L = 0.65\mathrm{Ra}^{-0.16\pm0.02}\mathrm{Pr}^{0.24\pm0.01}$.

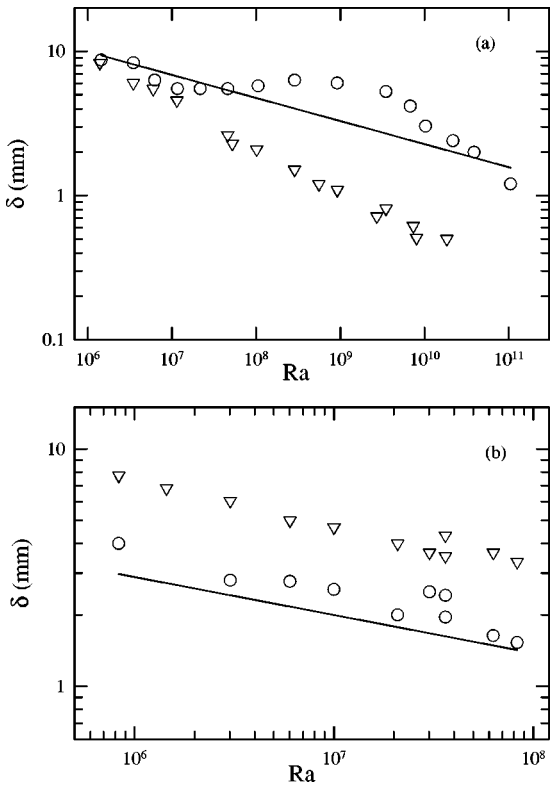

FIG. 4. Viscous boundary layer δ_v measured using the ''power spectra'' method and those extrapolated from Eq. (1) to the corresponding values of Pr and Ra: (a) gas data with Pr = 0.7 (Ref. [6]); (b) mercury data with Pr = 0.024 (Ref. [7]). In both cases, the solid lines are the extrapolations and circles are measured δ_v. The corresponding thermal layer thicknesses δ_{th} (inverted triangles) are also shown.

whether this method really measures δ_v has also been questioned [8]. Recently, Xia and Zhou have tested the ''power spectra'' method in water for two decades of Ra and the result is in good agreement with that from direct measurements [19]. But as far as Pr is concerned the test is inconclusive. We now compare δ_v given by Eq. (1) and those measured by the power spectra method. Figure 4 shows the viscous boundary layers (circles) and thermal boundary layers (triangles) measured in (a) high-pressure gas (Pr=0.7) [6] and (b) mercury (Pr=0.024) [7]. The solid lines in the figure are our result extrapolated to the corresponding values of Pr and Ra. For the Ra dependence, the data are too scattered for a quantitative comparison, and as an extrapolation our result is not able to say anything about the apparent transitions shown in the gas data. Nevertheless, the figure appears to show approximate agreement in the overall magnitude between the indirect results and extrapolated ones for two systems with very different values of Pr from ours. In our view, the fact that Eq. (1) is able to connect results from systems with widely separated Pr lends mutual support to the indirect technique and to the extrapolation. Thus our data appear to support the conclusions that the thermal and viscous layers have crossed in mercury [7] but not yet in gas [6]. Note that the boundary layer crossing in mercury was one of the arguments used in Ref. [20] to rule out the existence of the asymptotic, or ultrahard, regime in turbulent convection. However, one should use caution in interpreting the above result. For example, Grossmann and Lohse's recent theoretical result on the properties of the Nusselt number suggests that there may be a transition in the Pr dependence of Nu around Pr$\simeq$1 [21] and there appears to be experimental evidence to support it [22]. Since the lowest Pr for our measured δ_v is 6, we do not know whether a similar transition exists for the viscous boundary layer. Clearly, further investigations are needed and the above extrapolation results should be viewed more as a way to stimulate such efforts.

B. Reynolds number Re_{V_m} based on the maximum velocity

The Reynolds number $\mathrm{Re}_{V_m} = V_{max}L/\nu$ is based on the maximum velocity V_{max} of the horizontal velocity profiles near the bottom plate, as measured by the two-beam technique. Because Re_{V_m} for the low- and high-Pr fluids appear to have different behavior, we examine first the results from water that had been published previously but were presented in terms of the Peclet number Pe (=RePr) [5]. The water data were measured in four cells of varying aspect ratio $\Gamma = D/L$, where D is the cell diameter and L its height. Since the values of Pr for these data varied from 4.3 to 7, a plot of Re_{V_m} against Ra would be quite scattered. So we first determined the Pr dependence of these data by minimizing their scatter around straight lines (for each Γ in a log-log plot; the

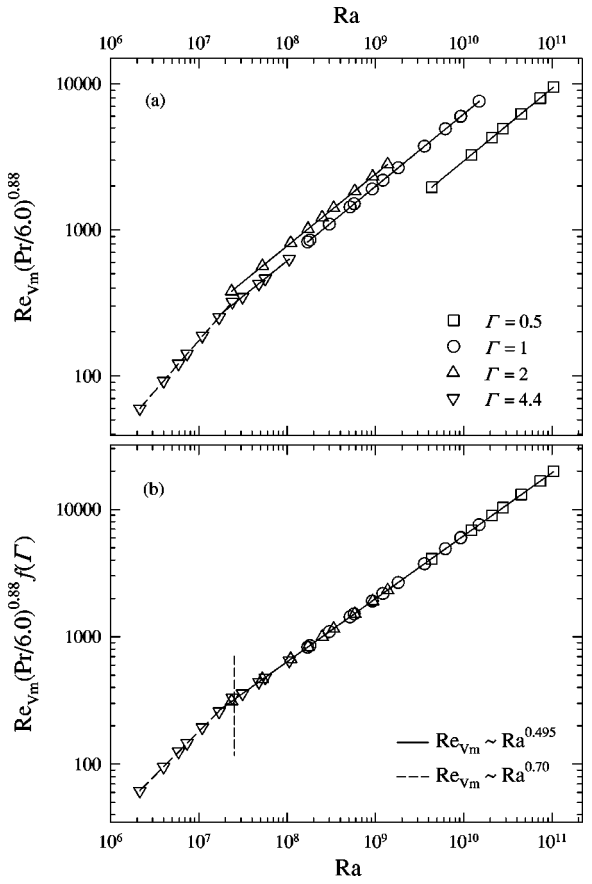

FIG. 5. (a) The Reynolds number Re_{V_m} measured in water from different aspect ratio cells. The data have been normalized to a constant Pr=6.0. (b) Data in (a) after the dependence on aspect ratio Γ is compensated by the factor $f(\Gamma)$ which depends only on Γ. In both (a) and (b), all solid lines have a slope of 0.495 and the dashed lines 0.70.

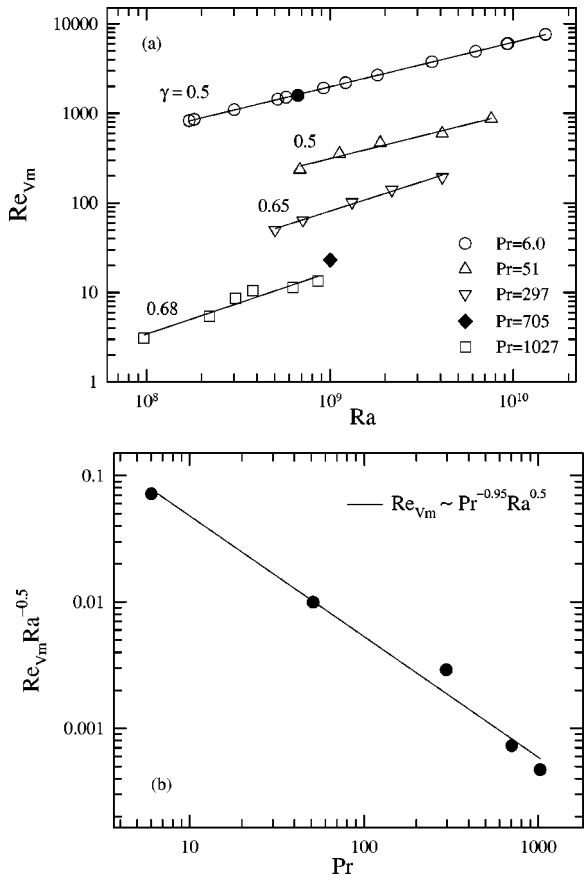

FIG. 6. (a) Re_{V_m} measured at different values of Pr plotted against Ra. As in Fig. 5, the water data are normalized to Pr=6.0, i.e., Re_{V_m} is multiplied by $(\mathrm{Pr}/6.0)^{0.88}$ for these data, and only those for $\Gamma=1$ are shown. The Ra exponent γ for each group of data is shown beside that group. (b) Data in (a) fitted with the same Ra exponent $\gamma=0.5$ for all and plotted as $\mathrm{Re}_{V_m}\mathrm{Ra}^{-0.5}$ vs Pr; the solid line has a slope of -0.95.

results show that $\mathrm{Re}_{V_m} \sim \mathrm{Pr}^{-0.88}$ for each set. We then normalized all the data to a constant Pr ($=6.0$); the results, plotted against Ra, are shown in Fig. 5(a). In the figure, all solid lines have a power-law exponent of $\gamma=0.5$ ($\mathrm{Re}_{V_m} \sim \mathrm{Ra}^{\gamma}$). Note that since the strong Pr dependence of Re leads to a weak Pr dependence of Pe, the effect of Pr was not considered in [5] and the same Ra dependence was obtained there. Still, we can see that the quality of the power-law fit in Fig. 5(a) is better than those shown in Ref. [5]. As Re_{V_m} shows no apparent systematic trend with Γ, we multiplied a function $f(\Gamma)$ by the normalized Re_{V_m} to extend the effective scaling range in Ra [$f(\Gamma)$ is a constant for each set of data and is chosen to collapse the data on a single line]. The results obtained are shown in Fig. 5(b) where a single power law $\mathrm{Re}_{V_m} \sim \mathrm{Ra}^{0.495}$ (solid line) for all data with $\mathrm{Ra} \geqslant 2\times10^7$ is produced [the symbols are the same as in Fig. 5(a)]. For data below Ra $\simeq 2\times10^7$, a power-law fit would give $\mathrm{Re}_{V_m} \sim \mathrm{Ra}^{0.70}$ [dashed line, which is also shown in Fig. 5(a)]. Note that $\mathrm{Ra} \simeq 2\times10^7$ corresponds roughly to the transition from soft to hard turbulence [23]. This transition was already seen in Ref. [5], but with the Pr dependence treated properly it becomes more pronounced here.

With the water data reanalyzed in terms of Re and their Pr dependence properly normalized, we compare them with data measured in this work from high-Pr fluids. These are shown in Fig. 6(a), where the solid lines represent the best power-law fit to the respective data and the obtained Ra exponents γ are indicated nearby (for clarity, only $\Gamma=1$ data from water are shown). Although the ranges of Ra are small for the high-Pr data, there appears to be a trend of γ increasing with Pr. For Pr=297, the difference between 0.65 and 0.5 appears to be beyond the uncertainties of the data. But for Pr=1027, the data scatter is sufficiently large [24] that we cannot rule out $\gamma=0.5$. In Fig. 6(a), the two solid symbols represent Re based on the maximum of the vertical velocity profiles near the sidewall as measured by the LDV (see Fig. 7). Because of the apparent lack of consistent Ra dependence for low- and high-Pr data, strictly speaking it is not meaningful to have a uniform Pr dependence for these data. But if we nonetheless want to check such a trend across a wide range of Pr, we need to use a single value of γ to

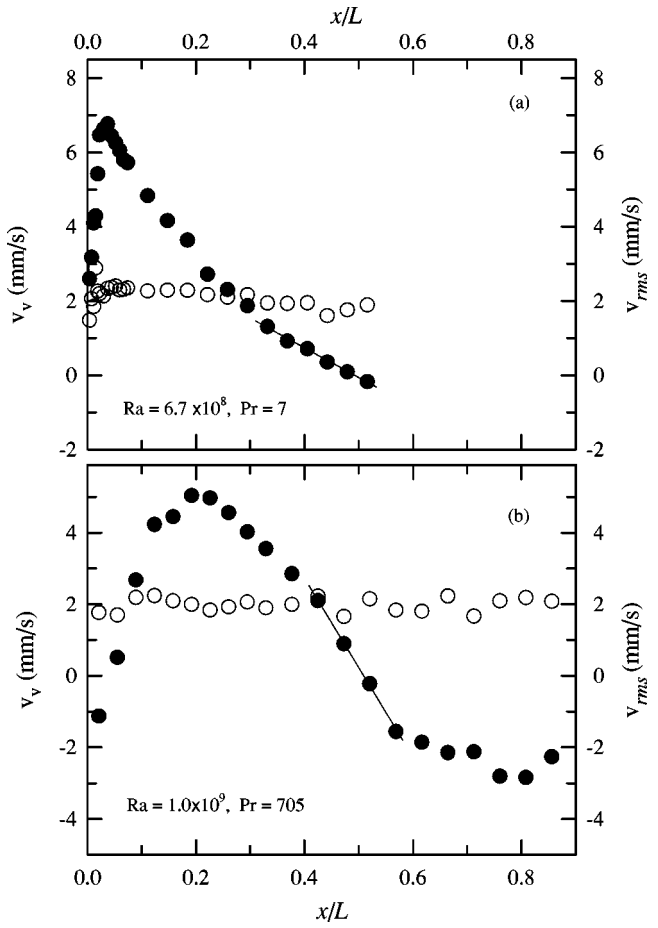

FIG. 7. Profiles of the mean (solid circles) and rms (open circles) values of the vertical velocity measured as a function of the horizontal distance x from the sidewall and at midheight from (a) water and (b) dipropylene glycol. The lines indicate regions of constant shear or linear velocity profile.

extract the trend (due to the sensitive dependence of amplitudes on exponents). This is done by fitting all the data with $\gamma=0.5$ and the amplitudes (which are essentially $\mathrm{Re}_{V_m}\mathrm{Ra}^{-0.5}$) are plotted against Pr in Fig. 6(b), where the solid line has a slope of -0.95. Recall that the Pr exponent is -0.88 for water, so this exponent seems to increase in absolute value with increasing Pr. A similar trend has been observed in numerical simulations by Verzicco and Camussi [25], who found that the Pr exponent of Re crosses over from -0.73 to -0.94 when Pr is increased. Interestingly, in a numerical study of convection in self-gravitating spherical shells, Tilgner also found [26] a similar crossover from -0.73 to -0.92. But in both cases, the crossover occurred around $\mathrm{Pr}\simeq 1$. In a recent theory, Grossmann and Lohse proposed to separate the energy and thermal dissipation into contributions from boundary layers and the bulk, and obtained a multitude of convection regimes in the Ra-Pr plane according to the relative weights of these components [1]. A specific prediction of the theory in the very large Pr regime [21] is a Nu independent of Pr and a Re strongly dependent on both Ra and Pr, i.e., $\mathrm{Nu}\sim\mathrm{Ra}^{1/5}\mathrm{Pr}^{0}$ and $\mathrm{Re}\sim\mathrm{Ra}^{3/5}\mathrm{Pr}^{-1}$. Our Re_{V_m} for the high-Pr data in Fig. 6 are seen to be showing a similar trend. In our view, the scaling result ($\gamma=0.7$) for the ''soft'' turbulence region in Fig. 5 may also belong to this regime, i.e., either high Pr or low Ra (see the ''phase diagram'' in Ref. [21]). But because of the small Ra range and somewhat noisy data from the high-Pr fluids, we would put this as tentative at best.

C. Reynolds number Re_o based on the oscillation frequency of the large-scale circulation

We now present results from LDV measurements. Profiles of the average and rms values of the vertical velocity from the sidewall to the interior of the cell (at midheight) were measured for a few values of Ra and Pr (but not systematically). Figure 7 shows two such profiles: (a) $\mathrm{Pr}=6.97$, $\mathrm{Ra}=6.7\times10^{8}$ and (b) $\mathrm{Pr}=705$, $\mathrm{Ra}=1.0\times10^{9}$. Note that (a) reaches only to the cell center whereas (b) is an almost complete profile. Similar to the horizontal velocity profiles near the bottom plate, the shapes of these profiles clearly change with Pr, which may be due to the non-Bousinessq nature of the high-Pr convection. Nevertheless, two features that were previously observed in water [27] are present in both cases: (i) the mean velocity $\overline{v}$ reaches a maximum near the sidewall and develops into a linear profile when it is less than v_{rms}; and (ii) v_{rms} is approximately constant in most parts of the cell. Using the maximum velocities in Fig. 7 we calculate the corresponding Reynolds numbers, which are shown as solid symbols in Fig. 6(a). It shows agreement for the measured magnitude of the large-scale circulation (LSC) using two techniques, albeit at only one point.

From flow visualizations, we found that the large-scale mean flow does not circulate constantly but goes through acceleration/deceleration cycles, which can also be seen from velocity time series [28]. The period f_o^{-1} of this oscillatory motion of the large-scale circulation can be obtained from the autocorrelation function of velocity fluctuations $C(\tau)=\langle\delta v(t+\tau)\delta v(t)\rangle/\langle(\delta v)^2\rangle$ ($\delta v=v-\overline{v}$). We find that f_o corresponds to the peak in the velocity power spectra but it can be more accurately determined from $C(\tau)$ (due to the former's uneven spectral point distribution on a logarithmic scale) [28]. Obviously, f_o is not the circulation frequency of LSC but the largest period of its coherent oscillations. We have previously found that f_o measured at various places in the cell is the same (except possibly in the boundary layers and cell center) [28] and thus provides a characteristic time scale of the system. We call it the global oscillation frequency of the LSC or the wind. Because of the apparent positional independence of both f_o and v_{rms}, the LDV measurements in which systematic variations of Ra and Pr are made did not take place at a fixed position but at positions about several centimeters from the sidewall (midheight) where $\overline{v}>v_{rms}$. Each measurement lasted for two hours; the mean and the rms velocities and the correlation functions are then calculated from the time series.

The inset of Fig. 8(a) shows an example of $C(\tau)$ for $\mathrm{Ra}=1.2\times10^{10}$ and $\mathrm{Pr}=37.8$ where the position of the first peak gives the value of f_o^{-1}. Using f_o one can define a Reynolds

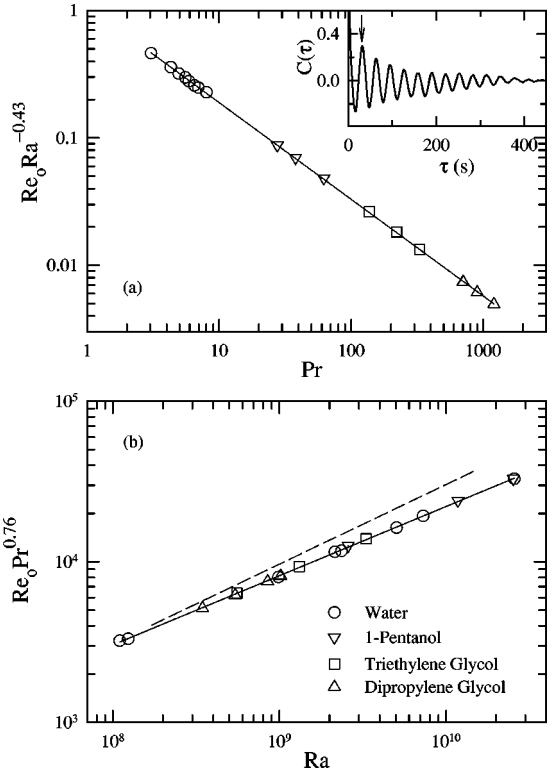

FIG. 8. Reynolds number Re_o based on the oscillation frequency f_o measured in different fluids at various Ra and Pr. (a) $Re_o Ra^{-0.43}$ vs Pr; the line has a slope of -0.76. The inset shows a velocity autocorrelation function vs the delay time τ measured at $Ra=1.2\times10^{10}$ and $Pr=37.8$. The arrow indicates the value of f_o^{-1}. (b) $Re_o Pr^{0.76}$ vs Ra, where the solid line has a slope of 0.43. The dashed line represents $Re_{V_m} Pr^{-0.88}=0.335Ra^{0.495}$ obtained from the water data in Fig. 5.

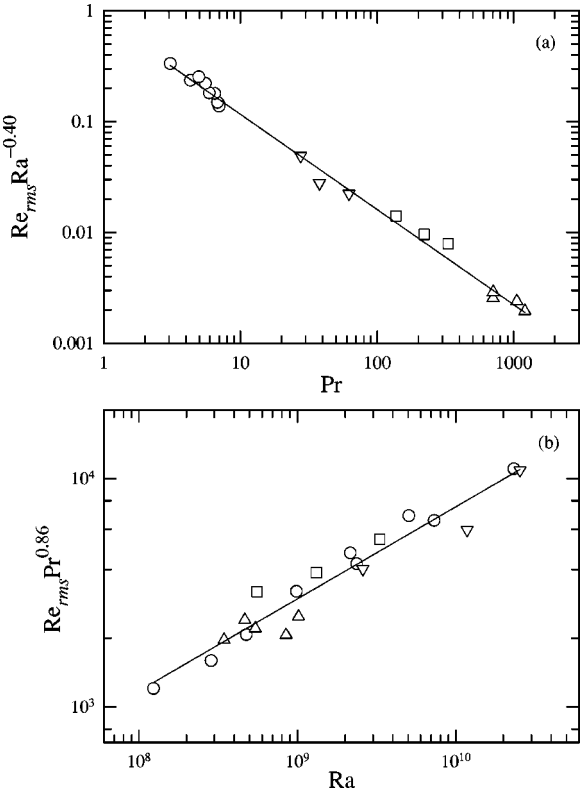

FIG. 9. The rms velocity based Reynolds number Re_{rms} measured at various Ra and Pr. (a) $Re_{rms} Ra^{-0.40}$ vs Pr, where the line represents a power-law fit with an exponent of -0.86. (b) $Re_{rms} Pr^{0.86}$ vs Ra, where the line has a slope of 0.4.

number $Re_o=4L^2 f_o/\nu$. Figure 8(a) shows $Re_o Ra^{-0.43}$ measured from the four fluids and plotted against Pr on a log-log scale [see Fig. 8(b) for symbol legends, which also apply to Fig. 9 below]. The varying range of Ra for these data is between 1.1×10^8 and 2.6×10^{10} and that of Pr is between 3.06 and 1,205, with the corresponding Re_o varying from 23.5 to 14 049. The exponent of 0.43 is determined by minimizing data scatter around a straight line; a power-law fit then gives $Re_o Ra^{-0.43}\sim Pr^{-0.76}$. Likewise, when Re_o is plotted against Ra on a log-log scale and data scatter is then minimized by multiplying Pr^{α} by Re_o, we obtain $\alpha=0.76$. This is shown in Fig. 8(b), where $Re_o Pr^{0.76}$ is plotted against Ra (open symbols); a power-law fit then gives $\sim Ra^{0.43}$ (solid line). Note that these two procedures are independent of each other and thus they showed a certain self-consistency. Combining the two results, we obtain $Re_o=1.09Ra^{0.43\pm0.01}Pr^{-0.76\pm0.01}$. (See below for a discussion on the dashed line.) Note that a similar result for Re_o was obtained previously over narrower ranges of Pr [29], where f_o was determined from the velocity power spectra.

D. Reynolds number Re_{rms} based on the local rms velocity

As mentioned above, our v_{rms} are not measured at the same position but nonetheless should be fairly representative of typical local velocity fluctuations for the entire system. Figure 9 shows the Reynolds number $Re_{rms}=v_{rms}L/\nu$ based on the local rms velocity as a function of Ra and Pr. In contrast to Re_o, Re_{rms} exhibits considerable scatter, although they come from the same set of data. This is probably due to a weak positional dependence of v_{rms} (from Fig. 7, we see that v_{rms} is only approximately constant with respect to position). It may also imply that while a two-hour averaging may have been sufficient for global quantities such as f_o it may not be enough for local quantities like v_{rms}. In Fig. 9, the power-law fitting $Re_{rms}=0.84Ra^{0.40\pm0.03}Pr^{-0.86\pm0.01}$ is deduced similarly as in Fig. 8. Because of the large data scatter, the Ra exponent has a large error bar, which leaves us unable to differentiate it from that for Re_o. On the other hand, the strong Pr dependence of Re_{rms} combined with a wide parameter range produces a smaller error bar for its Pr exponent, which appears to differ a lot from that of Re_o. While the Ra dependences of Re_{rms} and Re_o appear to be indistinguishable for the present data, the difference in their Pr dependence seems to be real (0.86 vs 0.76). It should also be noted that the strong Pr dependence of our measured Re_{rms} is in marked contrast to the findings from gas convection near the critical point [30], where Re_{rms} was found to be independent of Pr.

IV. SUMMARY

With δ_v(Ra,Pr) and the several Re(Ra,Pr) determined over a wide range of the control parameters, we now discuss

the implications of these results and make preliminary comparisons with some theoretical work. An important ingredient in the model by Grossmann and Lohse (GL) [1] is the assumption of a Blasius type laminar viscous layer $\delta_v/L = 1/[4\sqrt{(}\mathrm{Re})$, which is used to model the energy dissipation rate of the system. Using either Re_{V_m} or Re_o or even Re_{rms} and comparing it with Eq. (1), we find the above assumption is not supported by our data for either magnitude or the Ra or Pr dependence. This is so even though our viscous layer remains laminar for the highest Ra reached [31]. We note that the large mismatch in magnitudes (e.g., at $\mathrm{Pr}=7$ and $\mathrm{Ra}=1\times10^9$, $0.25\mathrm{Re}^{-1/2}$ is about seven times smaller than δ_v/L, for either Re_o or Re_{V_m}) will lead to an underestimate of the energy dissipation in the boundary layer region. Note that, however, in the GL theory, the same viscous layer is assumed for both the sidewall and the conducting plates [1]. In a previous experiment [14], Qiu and Xia measured the Ra dependence of the viscous layer at the sidewall and found $\delta_v \sim \mathrm{Ra}^{-0.26\pm0.03}$, which is consistent with the Blasius boundary layer assumption, at least for the Ra dependence, if the wind-based Reynolds number Re_{V_m} is used. No experimental result for the Pr dependence of δ_v at the sidewall is available at present. But, based on the Ra property of δ_v, it is reasonable to argue that it is probably different from that at the conducting plates. Thus, one may need to use two viscous boundary layers, one at the sidewall and one at the conducting plates, to model kinetic energy dissipation in a GL type theory in the future.

We now compare Re_{V_m} with Re_o and Re_{rms}. Since Re_{V_m} from the high-Pr fluids do not have enough precision, we use only the water data which, as mentioned above, can be represented as $\mathrm{Re}_{V_m}=0.335\mathrm{Ra}^{0.495}\mathrm{Pr}^{-0.88}$. This result is shown as the dashed line in Fig. 8(b) (i.e., $\mathrm{Re}_{V_m}\mathrm{Pr}^{0.88}$ vs Ra) along with Re_o. It is seen that for the given precision of the data (see Fig. 4 for the quality of Re_{V_m}), there appears to be a real difference between the two quantities and this difference should become more pronounced with increasing Ra. Another thing to be noted is that Re_o appears to have a more uniform behavior across the wide range of Pr than Re_{V_m} does, which can be taken as another sign that the two are different quantities. One is based on ''true velocity'' and the other is based on a certain time scale of the fluctuating velocity and appears to be related more to the rms velocity. We note that the prediction $\mathrm{Re}\sim\mathrm{Ra}^{3/7}\mathrm{Pr}^{-5/7}$ from an earlier scaling theory of Shraiman and Siggia [32] (the same Ra exponent was also obtained by Castaing *et al.* [33]) appears to be in excellent agreement with our measured Re_o and, to a lesser extent, Re_{rms}, as far as the Ra dependence is concerned. For the Pr dependence, the agreement is less good and more so for Re_{rms}. It is interesting that in Ref. [32] Re is based on the large-scale velocity, whereas in Ref. [33] it is based on the fluctuating velocity at the cell center. Our results for Re_o and Re_{rms} are also consistent with Kraichnan's prediction $\mathrm{Re}\sim\mathrm{Ra}^{4/9}\mathrm{Pr}^{-2/3}$, based on the rms velocity at the cell center [34], for the Ra part, although the Pr exponent has a larger deviation than in the more recent theories. As for Re_{V_m}, which is based on the maximum value of the wind, we are not aware of any theory that predicts a 1/2 exponent besides the ''free-fall'' type argument. One exception is the Kraichnan prediction $\mathrm{Reln Re}\sim\mathrm{Ra}^{1/2}\mathrm{Pr}^{-1/2}$ for the ultrahard regime, which is clearly not the present case. We note that there is a current debate on what should be the true value of γ (i.e., 0.43–0.46 or 0.5), or perhaps what should be the representative Re in Rayleigh-Bénard convection. For example, Qiu and Tong recently found $\gamma=0.45$ for a Peclet number based on the mean rotation rate of the wind [35], which is close to our Re_o but in principle should be closer to Re_{V_m} since, presumably, similar quantities are measured. Since a recent paper by Chavanne *et al.* [36] contains a fairly complete compilation of the various results, we will not attempt to cite all of them here. It is also not our intention to resolve this issue here, simply because more experiments are needed. In our view, measurements such as those shown in Fig. 7 need to be done in a systematic way (i.e., across a wide range of Ra at fixed Pr); such measurements should produce quantities like Re_{V_m} and Re_o simultaneously and under the same conditions, which will then allow us to make a more meaningful comparison.

To conclude, we have measured the profiles of the time-averaged horizontal velocity along the central vertical axis of the convection cell for values of Pr from 6 to 1027 and of Ra between 2×10^8 and 2×10^{10}. We find that the profiles measured at the same value of Pr but varying Ra appear to have an invariant shape. On the other hand, profiles measured at varying Pr but approximately the same Ra do not seem to have an invariant form (Figs. 2 and 7). From these profiles, we deduce the viscous boundary layer thickness $\delta_v(\mathrm{Ra},\mathrm{Pr})$ and the Reynolds number $\mathrm{Re}_{V_m}(\mathrm{Ra},\mathrm{Pr})$ based on the maximum value of the wind V_{max} in the convection cell. The viscous layer can be described by $\delta_v/L = 0.65\mathrm{Ra}^{-0.16\pm0.02}\mathrm{Pr}^{0.24\pm0.01}$. To our knowledge, there is no previous result for the Prandtl number dependence of the viscous layer, either experimental or theoretical. When this measured viscous layer thickness is extrapolated to the Pr values of gas and mercury, we find surprisingly good agreement, in terms of overall magnitude, with those obtained from the indirect temperature power spectra method. The Ra dependence of $\mathrm{Re}_{V_m}(\mathrm{Ra},\mathrm{Pr})$ appears to vary across the range of Pr covered, with the exponent γ changing from 0.5 to 0.68 as Pr increases from 6 to 1027 (Fig. 6). The Pr exponent of Re_{V_m} for the whole data set has a value of -0.94 but is -0.88 if only the lower-Pr (water) data are used for the fitting, again showing a trend of increasing (in absolute value) with increasing Pr. In contrast to Re_{V_m}, the global oscillation frequency based $\mathrm{Re}_o(\mathrm{Ra},\mathrm{Pr})$ shows a ''uniform'' dependence on both Ra and Pr across the parameter space spanned in the experiment (Pr from 3 to 1200 and Ra from 1.1×10^8 and 2.6×10^{10}; Fig. 8), i.e., $\mathrm{Re}_o = 1.09\mathrm{Ra}^{0.43\pm0.01}\mathrm{Pr}^{-0.76\pm0.01}$. We find that the Reynolds number $\mathrm{Re}_{rms}(\mathrm{Ra},\mathrm{Pr})$ based on the rms values of local velocity may be described as $\mathrm{Re}_{rms} = 0.84\mathrm{Ra}^{0.40\pm0.03}\mathrm{Pr}^{-0.86\pm0.01}$ (Fig. 9). While the noisy data produce a large uncertainty in the Ra exponent of Re_{rms}, its strong Pr dependence is unmistakable, which appears to con-

tradict an earlier finding [29] of a Pr-independent Re_{rms}. It is seen from the above that all three Reynolds numbers have strong dependence on Pr. This leads us to speculate that the variations in the value of γ from the different experiments could be due, at least in part, to contamination from the Re Pr-dependence since not all experiments are carried out at strictly constant Pr.

ACKNOWLEDGMENTS

We thank P. Tong and K. R. Sreenivasan for stimulating discussions. We also thank P. S. Leang for her assistance in data acquisition and gratefully acknowledge support of this work by the Research Grants Council of the Hong Kong SAR under Grant No. CUHK 4281/00P.

[1] S. Grossmann and D. Lohse, J. Fluid Mech. **407**, 27 (2000).
[2] J.J. Niemela, L. Skrbek, K.R. Sreenivasan, and R.J. Donnelly, Nature (London) **404**, 837 (2000).
[3] K.-Q. Xia, S. Lam, and S.-Q. Zhou, Phys. Rev. Lett. **88**, 064501 (2002).
[4] Y.-B. Xin, K.-Q. Xia, and P. Tong, Phys. Rev. Lett. **77**, 1266 (1996).
[5] Y.-B. Xin and K.-Q. Xia, Phys. Rev. E **56**, 3010 (1997).
[6] A. Belmonte, A. Tilgner, and A. Libchaber, Phys. Rev. Lett. **70**, 4067 (1993).
[7] A. Naert, T. Segawa, and M. Sano, Phys. Rev. E **56**, R1302 (1997).
[8] See, for example, B.I. Shraiman and E.D. Siggia, Physica D **97**, 286 (1996).
[9] These are $>99\%$ pure solvents purchased from Acros Organics, Ltd.
[10] F. Busse, J. Fluid Mech. **30**, 625 (1967).
[11] C.L. Yaws, *Chemical Properties Handbook* (McGraw-Hill, New York, 1999).
[12] S.-L. Lui and K.-Q. Xia, Phys. Rev. E **57**, 5494 (1998).
[13] K.-Q. Xia, Y.-B. Xin, and P. Tong, J. Opt. Soc. Am. A **12**, 1571 (1995).
[14] X.-L. Qiu and K.-Q. Xia, Phys. Rev. E **58**, 486 (1998).
[15] We achieve the density match between the glass spheres and the liquid by first spinning the suspension in a centrifuge and then drawing out the middle part of the suspension with a syringe needle after the liquid has settled for a long time.
[16] Because the large refractive index of the fluid (compared to water) causes bending of the laser beams, we are not able to position them very close to the surface of the plate where there is a large refractive index gradient. Thus we do not know whether the velocity profile in Fig. 1 will become linear inside the thermal layer ($z \simeq 1.5$ mm for the present one, which is also the lowest point measured).
[17] J. Zhang, S. Childress, and A. Libchaber, Phys. Fluids **9**, 1034 (1997).
[18] J. Zhang, S. Childress, and A. Libchaber, Phys. Fluids **10**, 1534 (1998).
[19] K.-Q. Xia and S.-Q. Zhou, Physica A **288**, 308 (2000).
[20] J.A. Glazier, T. Segawa, A. Naert, and M. Sano, Nature (London) **398**, 307 (1999).
[21] S. Grossmann and D. Lohse, Phys. Rev. Lett. **86**, 3316 (2001).
[22] G. Ahlers and X. Xu, Phys. Rev. Lett. **86**, 3320 (2001).
[23] F. Heslot, B. Castaing, and A. Libchaber, Phys. Rev. A **36**, 5870 (1987).
[24] The flow at this Pr is very slow, so even with very long averages the data still show large scatter.
[25] R. Verzicco and R. Camussi, J. Fluid Mech. **383**, 55 (1999).
[26] A. Tilgner, Phys. Rev. E **53**, 4847 (1996).
[27] X.-L. Qiu, S.H. Yao, and P. Tong, Phys. Rev. E **61**, R6075 (2000).
[28] X.-D. Shang and K.-Q. Xia, Phys. Rev. E **64**, 065301(R) (2001).
[29] S. Ashkenazi and V. Steinberg, Phys. Rev. Lett. **83**, 3641 (1999).
[30] S. Ashkenazi and V. Steinberg, Phys. Rev. Lett. **83**, 4760 (1999).
[31] The highest shear Reynolds number based on the boundary layer thickness, $\mathrm{Re} = U\delta_v/\nu$, reached in the experiment is about 200, whereas the critical value for instability is about 420 [see, for example, L.D. Landau and E.M. Lifshitz, *Fluid Mechanics* (Pergamon Press, Oxford, 1987)].
[32] B.I. Shraiman and E.D. Siggia, Phys. Rev. A **42**, 3650 (1990).
[33] B. Castaing, G. Gunaratne, F. Heslot, L.P. Kadanoff, A. Libchaber, S. Thomae, X.-Z. Wu, S. Zaleski, and G. Zanetti, J. Fluid Mech. **204**, 1 (1989).
[34] R.H. Kraichnan, Phys. Fluids **5**, 1374 (1962).
[35] X.-L. Qiu and P. Tong, Phys. Rev. E **64**, 036304 (2001).
[36] X. Chavanne, F. Chillà, B. Chabaud, B. Castaing, and B. Hébral, Phys. Fluids **13**, 1300 (2001).